On the Extent and Connectivity of Conical Intersection Seams and the Effects of Three-State Intersections

Joshua D. Coe, Mitchell T. Ong, Benjamin G. Levine, and Todd J. Martínez*

Department of Chemistry, Beckman Institute, and Frederick Seitz Materials Research Laboratory, University of Illinois at Urbana−Champaign, 600 South Mathews Avenue, Urbana, Illinois 61801

Received: July 9, 2008; Revised Manuscript Received: October 6, 2008

We discuss the connectivity of intersection spaces and the role of minimal energy points within these intersection spaces (minimal energy conical intersections or MECIs) in promoting nonadiabatic transitions. We focus on malonaldeyde as a specific example, where there is a low-lying three-state conical intersection. This three-state intersection is the global minimum on the bright excited electronic state, but it plays a limited role in population transfer in our ab initio multiple spawning (AIMS) simulations because the molecule must traverse a series of two-state conical intersections to reach the three-state intersection. Due to the differences in seam space dimensionality separating conventional (two-state) and three-state intersections, we suggest that dynamical effects arising *directly* from a three-state intersection may prove difficult to observe in general. We also use a newly developed method for intersection optimization with geometric constraints to demonstrate the connectivity of all the stationary points in the intersection spaces for malonaldehyde. This supports the conjecture that all intersection spaces are connected, and that three-state intersections play a key role in extending this connectivity to all pairs of states, e.g. the S_1/S_0 and S_2/S_1 intersection spaces.

1. Introduction

Light-mediated chemistry offers the prospect of revolutionary and diverse applications such as coherent control,[1,2] rationally designed molecular scale devices,[3−5] and efficiently harnessing solar energy.[6] Progress in any of these endeavors requires understanding the evolution and decay of electronically excited states. Almost from the advent of quantum mechanics, it was known that Born−Oppenheimer surfaces[7] become nearly degenerate at select nuclear configurations.[8] Such points, dubbed avoided crossings, rightfully were identified closely with electronic relaxation. Soon after, it was realized that for polyatomic molecules there may also exist geometries where the energy gap vanishes completely.[9] These conical intersections,[10,11] nuclear configurations for which a pair of electronic surfaces becomes perfectly degenerate, have come to play a pivotal role in most discussions of electronically excited states.[3,12−14]

It is well-known that conical intersections are not isolated points, but rather high-dimensional "seams". Visualization of these high-dimensional objects is very difficult. Thus they often have been characterized by one or more representative lowest energy points within the "intersection space", molecular configurations known as minimal energy conical intersections (MECIs). The relevance of such geometries to electronic excited state dynamics has been a recurring question—can these MECIs be considered the analogues of transition states, i.e., bottlenecks in the electronic quenching from an electronic state to one lower in energy? Or is it instead necessary to consider the geometry of the entire intersection space? An additional wrinkle has been introduced by the recent realization that not only two-state conical intersections, but also three-state conical intersections (geometries where three electronic states become degenerate) are often accessible at energies below the Franck−Condon point.[15−20] How does the presence of three-state intersections affect electronic quenching dynamics and the topology of the intersection space?

Perhaps the first question to answer regarding intersection space topology relates to connectivity. We have conjectured previously[21] that all MECIs connecting a pair of electronic states are reachable by all other MECIs (connecting the same pair of electronic states) through a path lying entirely *within* the intersection space. In other words, that the intersection space for a given pair of states is fully connected. We have further hypothesized that three-state intersections play a key role in extending this "connectivity conjecture" to intersection spaces joining *any* pair of electronic states. Under these circumstances, the *entire* intersection space is fully connected, e.g., points lying on the S_0/S_1 seam are reachable from points lying on the S_2/S_1 seam via paths that link the two intersection spaces through three-state $S_2/S_1/S_0$ conical intersections. Ultimately, a rigorous proof (or disproof) of this conjecture is desirable. However, until such a proof is available, explorations of intersection space connectivity provide evidence for the veracity of the conjecture.

In this paper, we use malonaldehyde as a test case in which to probe these issues. Malonaldehyde is the paradigmatic molecule for excited state intramolecular proton transfer (ESIPT), an important and well-studied photochemical process in its own right.[22−30] However, our present interest centers more on[19,20,31] (1) there existing two chemically distinct conical intersections thought to be relevant to decay of the S_2 bright state in this molecule, (2) one of these intersections being a low-lying three-state $S_2/S_1/S_0$ intersection that is also the lowest energy point on S_2, and (3) the molecule being small enough to permit extensive sampling.

The content of the present work is 3-fold. First, we use ab initio multiple spawning (AIMS) dynamics to examine the correlation of population flow with distance from the seam minimum. The potential dynamical relevance of a seam's extent, in addition to its point of minimal energy, has been noted previously,[10,32−34] and intersection of the seam space with the

* Address correspondence to this author.

10.1021/jp806072k CCC: $40.75
Published on Web 11/14/2008

steepest descent pathway on the upper electronic surface can promote relaxation "localized" at segments of the seam other than its minimum.[35] The present work enlarges upon this theme, and shows, surprisingly, that *neither* of the above-mentioned conical intersection geometries (which are stationary points within the seam space) provides a good representation of geometries leading to nonadiabatic transitions. This contrasts sharply with the common portrayal of MECIs as the dominant locus of quenching along a seam.

Second, we link two conical intersection extrema of very different chemical character without breaking the degeneracy at any point along the connecting pathway using a recently developed intersection optimization method incorporating geometric constraints. This allows us to show that only one of these points is truly an MECI—the other is an intersection space saddle point whose precise order has yet to be determined.[33,36,37]

Finally, we examine the extent to which 3-state intersections participate *directly* in electronic relaxation. After clarifying the relative significance of the minimal energy three-state intersection (ME-3SI) for $S_2 \rightarrow S_1$ internal conversion in malonaldehyde, we examine its role in ground state recovery. Although three-state intersections in methyl cation[38] were examined much earlier, recent discussions canvas their occurrence in ethyl,[16] allyl,[17,39] and pyrazolyl radicals,[18,40−44] butadiene,[45] and the nucleic acid bases cytosine,[46,47] uracil,[15] and adenine.[15] General analysis of the seam space,[41,42] geometric phase,[39,48] and algorithms for 3-state seam minimization[16,45] have also been reported. Apart from a single preliminary study,[19] however, exploration of the role played by three-state intersections in the context of molecular dynamics has been lacking.

What follows is a series of observations regarding conical intersections and their role in nonadiabatic dynamics of polyatomic molecules. Although points are adduced from evidence in malonaldehyde, we believe that underlying each are principles whose validity can be extended to many other systems with only minor modification.

2. Methods

Intersection connectivity is demonstrated by using an optimization scheme detailed previously,[45,49] but adapted to include geometric constraints. The algorithm utilizes a Lagrange multiplier penalty method,[50] and is able to locate minima along an intersection seam without knowledge of the nonadiabatic coupling vector. Derivative discontinuities are smoothed with a penalty function G, which remains smooth even in the neighborhood of a discontinuity in the gradient of the potential surface. The objective function to be minimized is:

$$L_{IJ}(\mathbf{R};\sigma,\lambda,\alpha) = \bar{E}_{IJ}(\mathbf{R}) + \frac{1}{2}\sigma G(\Delta E_{IJ}(\mathbf{R});\alpha) + \sum_{n=1}^{N_{geo}} \lambda^{(n)}(\varphi^{(n)}(\mathbf{R}) - \varphi_0^{(n)}) \quad (1)$$

where I and J label electronic states with average energy $\bar{E}_{IJ}$ and energy difference ΔE_{IJ}, $\mathbf{R}$ denotes the full range of molecular coordinates, and $\varphi^{(n)}(\mathbf{R})$ denotes one of the N_{geo} internal coordinates that is to be constrained to the value $\varphi_0^{(n)}$. The Lagrange multipliers $\lambda^{(n)}$ enforce the geometric constraints, the smoothing parameter α ensures well-behaved surfaces even near conical intersections, and σ is a sequentially updated parameter driving the optimization toward the seam space minimum. In the work discussed here, we constrain a single dihedral angle (φ_{ijkl}) spanning atoms i, j, k, and l to the value φ_0, but adaptation to bond or angle constraints is obvious. Use of the smoothing function G is similar in spirit to Yarkony's use of extrapolatable functions,[51,52] but his are within the context of a Newton−Raphson scheme requiring nonadiabatic couplings and Hessian updating. The specific form of G used in the present work is

$$G = \frac{\Delta E_{IJ}^2}{\Delta E_{IJ} + \alpha} \quad (2)$$

A great deal of additional detail, including extension to three-state and minimal distance conical intersections (the "nearest" intersection according to some distance metric, such as rmsd), has been given previously.[45] Alternate methods for mapping the intersection seam have also appeared recently.[33,36,37,53,54]

Complete active space self-consistent field (CASSCF)[55] with a (4/4) active space and a 6-31G* basis set was employed both for intersection optimization and ab initio dynamics. Orbitals were state-averaged[56,57] with equal weights. This level of treatment was benchmarked extensively for malonaldehyde in previous work,[20] and shown by its consistency with multireference singles and doubles configuration interaction (MR-SDCI) benchmarks to provide a faithful representation of the excited state potential energy surfaces (PESs). All electronic structure calculations were carried out with the MolPro package.[58]

Nonadiabatic molecular dynamics was performed with the ab initio multiple spawning (AIMS) technique, implemented within MolPro.[59] AIMS employs an adaptive basis set of frozen Gaussians[60] following classical trajectories to sample the appropriate phase space. At points of significant nonadiabatic coupling, the basis set is dynamically enlarged to allow for transfer of population between electronic states. When a new basis function is created, or "spawned", its coefficient is coupled to that of its "parent" through the time-dependent Schrödinger equation (TDSE). The AIMS wave function for *NStates* electronic states is given as:

$$\Psi_{AIMS}(\mathbf{R},\mathbf{r},t) = \sum_{I}^{NStates} \Psi_{AIMS}^{I}(\mathbf{R},\mathbf{r},t) \quad (3)$$

where $\mathbf{R}$ and $\mathbf{r}$ denote nuclear and electronic coordinates, respectively. The wave function for each electronic state is represented as a sum of N_I complex, time-dependent Gaussians χ_j^I having complex, time-dependent coefficients c_j^I. The Gaussians themselves are parametrized by mean positions $\bar{\mathbf{R}}$, momenta $\bar{\mathbf{P}}$, fixed widths $\boldsymbol{\alpha}$, and phase γ:

$$\Psi_{AIMS}^{I}(\mathbf{R},\mathbf{r},t) = \sum_{j}^{N_I(t)} c_j^I(t)\chi_j^I(\mathbf{R},t;\bar{\mathbf{R}}_j^I,\bar{\mathbf{P}}_j^I,\alpha,\gamma_j^I)\phi_I(\mathbf{r};\mathbf{R}) \quad (4)$$

where ϕ_I is the wave function for the Ith adiabatic electronic state. The evolution of $\bar{\mathbf{R}}_j^I$ and $\bar{\mathbf{P}}_j^I$ follows the classical equations of motion corresponding to the Ith electronic state. The necessary forces are obtained by solving the electronic Schrödinger equation at each of the points $\bar{\mathbf{R}}_j^I$ for each time step. Thus, each of these multidimensional trajectory basis functions (TBFs) evolves on a single adiabatic electronic state, and the limit N_I on the sum in eq 4 increases as new basis functions are created, i.e. "spawned," on the Ith electronic state. The TBFs are products of one-dimensional Cartesian Gaussian functions with time-independent widths,

$$\chi_j^I = e^{i\gamma_j^I t}\prod_{\rho=1}^{3N} e^{-\alpha_\rho(R_\rho - \bar{R}_{j\rho}^I)^2 + i\bar{P}_{j\rho}^I(R_\rho - \bar{R}_{j\rho}^I)} \quad (5)$$

where ρ labels the individual Cartesian coordinates of the nuclei. The coefficients c_j^I are propagated with the TDSE, and the TBF

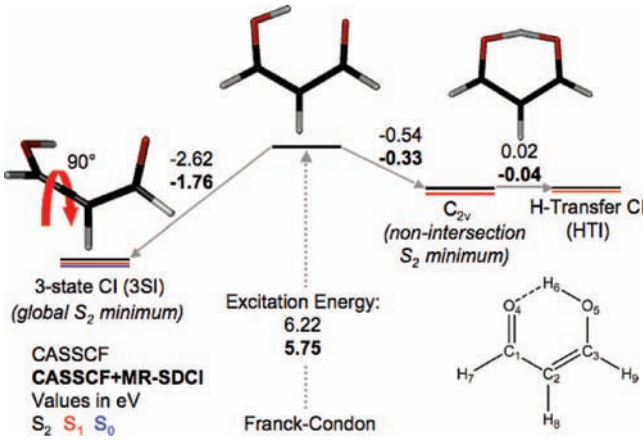

Figure 1. Stationary points of the SA3-CAS(4/4)/6-31G* S_2 potential surface. Energy differences in bold are taken from MR-SDCI energies at the CASSCF-optimized geometries. Following excitation in the FC region, there are two pathways for relaxation through conical intersection with S_1. The first of these involves torsion about the C_1-C_2 bond (see lower right for labeling convention), leading to a three-state intersection and quenching of excited state proton transfer (ESIPT). The other is closely coupled to ESIPT, and its minimal energy intersection differs from the ESIPT transition state (C_{2v}) only by slight displacement of H_8. The C_{2v} geometry represents the nonintersection minimum of S_2.

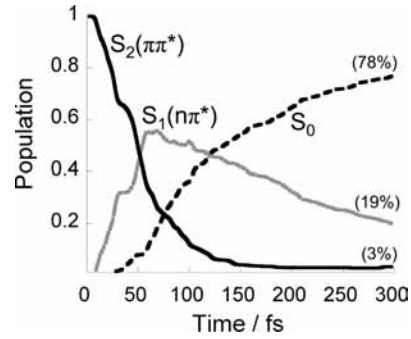

Figure 2. AIMS population dynamics for malonaldehyde, computed at the SA3-CAS(4/4)/6-31G* level. Rapid depletion of the spectroscopic state (S_2) results in the experimentally reported broad and featureless absorption spectrum, while significant ground state recovery within 300 fs prevents observation of fluorescence as also has been reported experimentally. Branching ratios at the close of the simulation are given in parentheses.

phase evolves semiclassically (as the time-integral of the Lagrangian). Additional detail can be found in previous review articles.[61,62] For the present work, it is especially important to note that we can define the weight or "population" of any of the TBFs in a manner analogous to the Mulliken definition[63] for electronic basis functions:

$$n_j^I = \sum_i^{N_I(t)} \mathrm{Re}((c_i^I)^* S_{ij} c_j^I) \qquad (6)$$

where S_{ij} is the overlap matrix element between a pair of Gaussian basis functions.

Nuclear basis function widths were chosen as discussed previously,[61] and the specific values used here are 30 and 6 bohr^{-2} for C/O and H atoms, respectively. Initial conditions for the TBF centroids were sampled randomly from the Wigner distribution[64] corresponding to the ground vibronic state in the harmonic approximation. The initial basis set consisted of 128 TBFs, which after 300 fs of simulation had grown to almost 5000. The S_0 minimum geometry and frequencies used to generate the Wigner distribution are obtained by using MP2 with a 6-31G* basis set.

3. Conical Intersections in Malonaldehyde

We first summarize some of the important geometries in the excited state dynamics of malonaldehyde, as detailed previously.[20] The geometries shown in Figure 1 were optimized at the CASSCF level, but energy differences computed with CAS(4/4)-SDCI at the CAS-optimized geometries are also provided (bold) for comparison. Following excitation to $S_2(\pi\pi^*)$, which is the lowest optically bright excited state, there are two alternate and potentially overlapping decay pathways. Each of these is characterized by a chemically distinctive S_2/S_1 minimal energy conical intersection, located with a standard optimization procedure.[65] The first of these requires little distortion from the Franck−Condon point and has C_s (almost C_{2v}) symmetry. Due to its geometric resemblance to the hydrogen transfer transition state on S_0, we labeled it the hydrogen transfer intersection (HTI). The second intersection is much lower in energy, a twisted geometry linking the first *three* singlet states, i.e. an $S_2/S_1/S_0$ ME-3SI.[19] This ME-3SI represents the global minimum on S_2 in malonaldehyde.

An additional S_1/S_0 MECI can be reached by simple linear interpolation starting from the ME-3SI, without breaking the S_1/S_0 degeneracy at any of the intervening points. Linkage of these points, demonstrated without attempt to optimize the connecting pathway, raised the prospect of extending the seam to the HTI as well, thereby connecting all of the optimized intersections among the first three singlet states. Similar mappings of seam spaces in ethylene,[66] fulvene,[36] and cytosine[47] have been described previously. Linkage of the HTI and ME-3SI would be much more surprising than the connection of the ME-3SI and S_1/S_0 MECI. The ME-3SI and HTI geometries are, chemically speaking, quite dissimilar.[20] The S_1/S_0 MECI and ME-3SI are quite similar and differ only by pyramidalization of a carbon atom. In contrast, the HTI is planar along the molecular backbone and hydrogen bonded across the mouth of the chelate ring. These differences are also reflected energetically—the ME-3SI and S_1/S_0 MECI differ in energy by only ~0.25 eV, whereas the difference in energies of the ME-3SI and HTI is well in excess of 2 eV. As mentioned above, demonstrations of connectivity here and elsewhere[33,36,66−70] feed speculation[21] that the locus of all intersection points within a molecule comprises a smooth, closed path in configuration space (possibly dissociative along some axes). According to the strongest form of this universal connectivity hypothesis, pairs of states are linked through 3-state intersections, which then assume a pivotal role in shaping the full manifold of electronically excited states.

4. Results and Discussion

A. Electronic Relaxation and Intersection Extrema. AIMS population dynamics for the ensemble described above is shown in Figure 2. The lifetime of the spectroscopically bright state (S_2) is extremely brief (≈60 fs), ensuring the observed broad and featureless absorption spectrum.[71] An intermediate dark state also exhibits a very short lifetime of roughly 175 fs, consistent with the lack of observed fluorescence.[72] At the close of 300 fs, almost 80% of the population has already made its way back to the ground state. Although the experimental data are limited in scope, those which are available are consistent with the decay rates predicted by AIMS.

As mentioned above, there are two optimized intersections that could be involved in the population loss from S_2. The

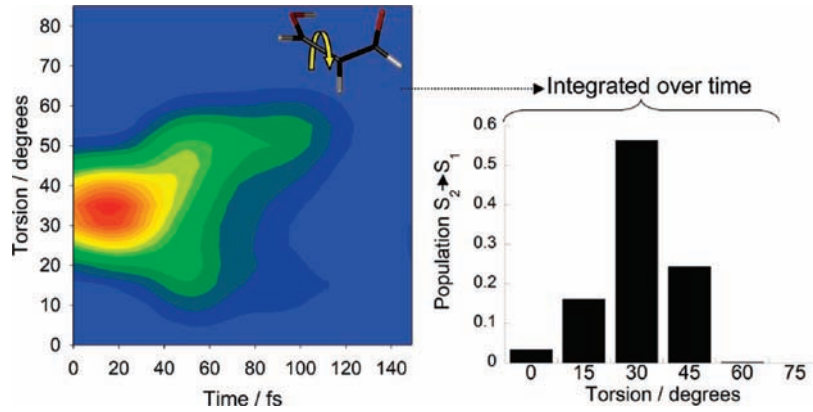

Figure 3. Left panel: Two-dimensional representation of $S_2 \rightarrow S_1$ nonadiabatic population transfer as a function of time and torsional angle (depicted in inset). Data have been convoluted in both dimensions as described in the text. Red indicates large values of population transfer and light blue indicates zero population transfer. The procedure used for binning nonadiabatic events is described in the text. Right panel: $S_2 \rightarrow S_1$ population transfer as a function of torsional angle only, illustrating that the bulk of electronic relaxation occurs away from both the HTI (0°) and the ME-3SI (90°).

prospect of competition between these two decay channels is interesting given the large differences in energy, geometry, and electronic character (chemistry) of their end points. As we have detailed previously,[20] torsion dominates and the full extent of ESIPT rises only to ~20%. However, on the basis of these two stationary points within the S_2/S_1 intersection space, one still expects to find population transferred in "clumps" surrounding torsional angles of 0° and 90°.

Testing this hypothesis requires a means of assigning molecular properties, such as torsional angles, to population transfer events ("spawning regions", in the language of AIMS) of individual TBFs. Because population transfer takes place over an extended region of nonadiabatic coupling and a finite time span, population transfer events encompass a range of molecular geometries, energies, etc. Characterizing these extended regions by unique values of some property X amounts to a coarse graining procedure, requiring selection of appropriate points at which to sample. We mark the beginning of an event by population loss from a basis function of 0.5% or greater over the course of a single time step, and its end when this same quantity drops below 0.1%. The total population lost during this time is denoted as Δn. Variables within this interval are assigned unique values $X_{\Delta E_{\min}}$, coinciding with their value at the time $t_{\Delta E_{\min}}$when the energy gap between the interacting electronic states reaches a minimum value $\Delta E_{\min}$. Typically, this coincides with the point of maximum nonadiabatic coupling over the course of the event. Generalizing to an ensemble of N_{bf} basis functions, each encountering N^i_{events} nonadiabatic events with associated population loss Δn, the amount $P_{1\rightarrow 2}$ of population transfer binned at time t and variable value X becomes

$$P_{1\rightarrow 2}(X,t) = \sum_{i=1}^{N_{\text{bf}}} \sum_{j=1}^{N^i_{\text{events}}} \Delta n_{ij} \delta(t - t^{ij}_{\Delta E_{\min}}) \delta(X - X^{ij}_{\Delta E_{\min}}) \quad (7)$$

To compensate for the discrete character of the data, the histogramming results reported below were convoluted with Gaussians having a full width at half-maximum of 30 fs in time and either 15° in angle or roughly 0.5 eV in energy.

Given this procedure for assigning a "location" to transfer of population between electronic states, we examine first the competition between $S_2 \rightarrow S_1$ quenching through the HTI versus that at the 3SI by assigning torsional angle values to each population transfer event of the TBFs. As evidenced by the results shown in Figure 3, the prediction of a bimodal distribution, biased toward 90°, is not even qualitatively correct. Relatively little population is transferred near either of the S_2 intersections, and none of it occurs anywhere close (geometrically) to the true S_2/S_1 MECI (the ME-3SI). Rather than clustering at 0° and 90°, values are distributed over the 15−60° range and concentrated between 30° and 45°. No population transfer takes place at torsional angles greater than 60°, and very little (<5%) occurs at angles less than 15°. In addition to highlighting the fact that torsion proceeds very rapidly, these facts raise the interesting question of why, if the S_2/S_1 MECIs fall at 0° and 90°, does no population transfer occur in the immediate neighborhood of those geometries?

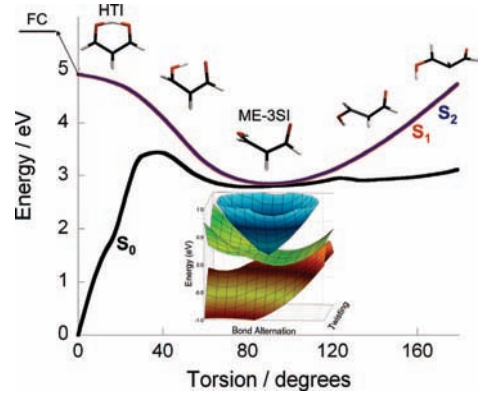

Figure 4. Connectivity of the hydrogen transfer (HTI) and minimal energy 3-state intersection (ME-3SI) points. Constrained relaxation in 5° intervals from the planar to 90° twisted geometries maintains the degeneracy of S_2 with S_1 at all points along the connecting pathway. The Franck−Condon (FC) point is located at 0° torsion, slightly higher in energy than the HTI. The inset shows an approximate view of the surface topography in the vicinity of the ME-3SI.

The answer lies in remembering that conical intersections comprise $(N - 2)$-dimensional seams, not isolated points of measure zero. The intersection geometries shown in Figure 1 merely mark points on a hyperplane cutting through the full configuration space of the molecule. The point is made more forcefully by tracing a path along this hyperplane, as in Figure 4. The path was generated by using the constrained optimization procedure described above, marking points along the seam in 5° intervals of the $\varphi_{O_4C_1C_2C_3}$ torsional angle (see Figure 1). The electronic energy of S_0 gradually increases along this path proceeding from the planar geometry and becomes degenerate with S_1 and S_2 at the ME-3SI. The HTI is an intersection of

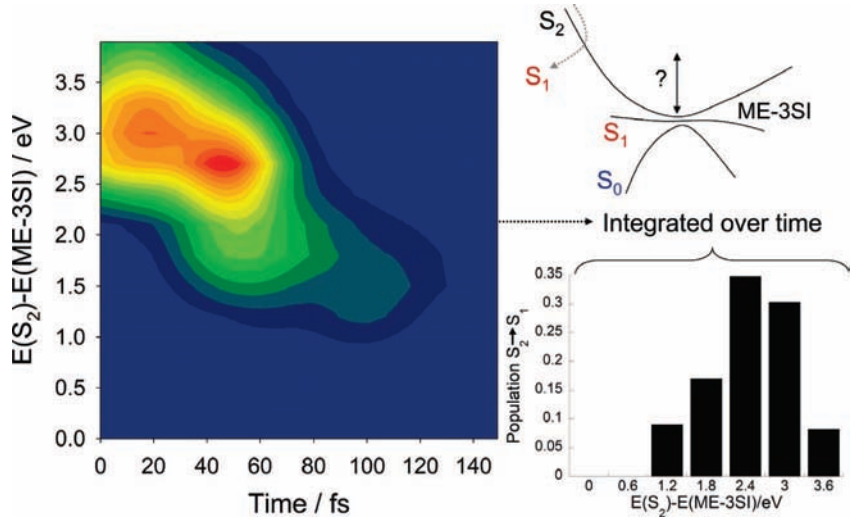

Figure 5. Left panel: Two-dimensional representation of $S_2 \rightarrow S_1$ nonadiabatic population transfer as a function of time and energy in excess of the ME-3SI. Data have been convoluted in both dimensions as described in the text. Right panel: $S_2 \rightarrow S_1$ population transfer as a function of excess energy only, illustrating that all electronic relaxation occurs at energies well above that at the ME-3SI.

states having $n\pi^*$ and $\pi\pi^*$ character. As discussed previously,[19,20] the ME-3SI arises from stabilization of the doubly excited ($\pi^*\pi^*$) state induced by torsional rotation, motion which also destabilizes the ground ($\pi\pi$) state. If the energy of the $n\pi^*$ state, which is less affected by torsion, lies roughly halfway between that of the ground ($\pi\pi$) and doubly excited ($\pi^*\pi^*$) states in the Franck−Condon region, then a 3SI will likely arise near the 90° twisted geometry. Other coordinates in addition to torsion must be modified in order to maintain degeneracy of S_1 and S_2 as one moves along the seam from the HTI to the ME-3SI. While S_1 is well-described as $n\pi^*$ throughout, S_2 changes from $\pi\pi^*$ to $\pi^*\pi^*$, with the latter becoming dominant at ∼45° torsion. Figure 4 indicates that the HTI is a saddle point in the S_2/S_1 seam space, the ME-3SI is the true minimum of the S_2/S_1 seam space, and between them lies a range of energetically accessible intersections leading away from the Franck−Condon region. Rigorous classification of the order of the saddle point in the intersection space for the HTI requires application of second-order methods for characterizing seam points in terms of mode frequencies. Such methods have recently been introduced,[70,73−77] but we have yet to apply them to malonaldehyde. However, it is likely that the HTI is a first-order saddle point in the intersection space, connecting the two symmetry-equivalent ME-3SIs corresponding to clockwise and counterclockwise torsion about the C−C bond. The seam continues for torsional angles from 90° to 180°. Many of these features strongly resemble those in *Z*-penta-3,5-dieniminium (ZPD), a model retinal chromophore. As with malonaldehyde, the planar intersection in ZPD is a saddle point in the S_1/S_0 seam space,[33] and surface hops[78] between states are concentrated at torsional angles of 60−80° as opposed to the (∼90° twisted) seam minimum.[35] The seam persists for torsional angles spanning the full range 0−180°.[36]

Because discussion of intersection seams, for ease of calculation and visualization, frequently devolves into detailed consideration of their minima, it is useful to probe further the extent to which the ME-3SI typifies molecular properties at points of significant $S_2 \rightarrow S_1$ relaxation. It is clear that, geometrically speaking, population transfer occurs nowhere close to the ME-3SI, but how about energetically? How similar is the potential energy at points of significant internal conversion to that at the ME-3SI? This question is addressed in Figure 5, where the same procedure as was applied to torsion is applied to the "excess" energy, the difference in the energy of S_2 at population transfer points and at the ME-3SI. As is to be expected, energetic and geometric proximity to the ME-3SI are correlated, and the energetic distance decreases in time as did the geometric distance—the wavepacket is moving "downhill". Nevertheless, the wavepacket moving on S_2 comes no closer than 1.2 eV to the ME-3SI (Figure 5) prior to population being lost almost completely to S_1.

Extending the view of intersection connectivity to include a vibration roughly orthogonal to torsion offers further insight into depletion of S_2 prior to the wavepacket reaching the ME-3SI. Because $\pi \rightarrow \pi^*$ excitation typically excites bond alternation modes, an idealized version of such a coordinate (Figure 6, left) was chosen; the resulting two-dimensional view of the seam is shown in the right panel of Figure 6. The orthogonal displacement corresponds roughly to a branching plane[79] vector of the ME-3SI,[20] and is also closely related to a branching plane vector of the HTI (see Supporting Information of ref 19). Insomuch as it projects onto the branching space at any given point along the seam, it will break the degeneracy to first order in displacement. Due to the higher frequency of bond alternation modes relative to torsion (∼1500 cm^{-1} vs ∼300 cm^{-1}), the two-state intersection line is traversed multiple times as the molecule twists its way to the ME-3SI, indicated schematically by the yellow line in Figure 6. These repeated passes fully deplete S_2 population prior to S_0 becoming energetically accessible.

B. Electronic Relaxation and 3-State Intersections. Having established that the ME-3SI is not accessed on S_2 prior to its depletion, it would be tempting to assume that 3-state intersections therefore play no part in electronic relaxation. This assumption, however, falls prey to the same oversimplification that erroneously predicts $S_2 \rightarrow S_1$ population transfer to be localized in clusters around the HTI and ME-3SI. Just as the S_2/S_1 intersection seam cannot be reduced to two points, so the 3-state intersection seam cannot be reduced to one point. The wavepacket's failure to reach the ME-3SI does not imply that population does not transfer near 3-state intersections located higher in energy.

To clarify this point, eq 7 was applied again to $S_2 \rightarrow S_1$ nonadiabatic coupling regions, but this time binning the energy gap separating S_1 from S_0. If $S_2 \rightarrow S_1$ population transfer occurs when the S_1/S_0 gap is small, one can conclude that S_2 relaxation occurs in the vicinity of a three-state intersection. In fact, the

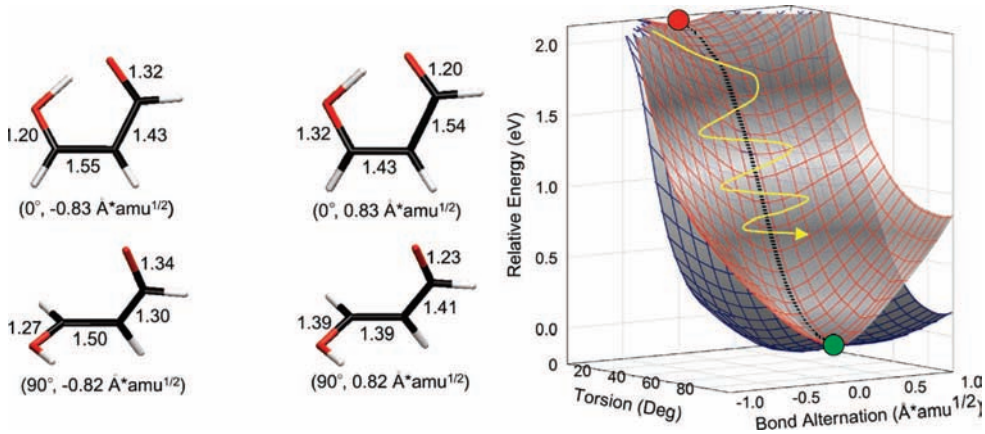

Figure 6. Two-dimensional view of the S_2/S_1 intersection seam connecting the HTI (red circle, top) and the ME-3SI (green circle, bottom). Perturbations along a bond alternation coordinate (illustrated at left) have been made to seam geometries along the torsional line shown in Figure 4 (depicted as a dotted line here). Because bond alternation projects onto one of the branching plane axes of both the HTI and ME-3SI, the degeneracy is broken to first order for displacements along this axis. The S_0 electronic state has been omitted for clarity, but intersects with S_2 and S_1 at the ME-3SI. The yellow line indicates a schematic of the observed dynamics that criss-crosses the seam as the molecule relaxes toward the ME-3SI.

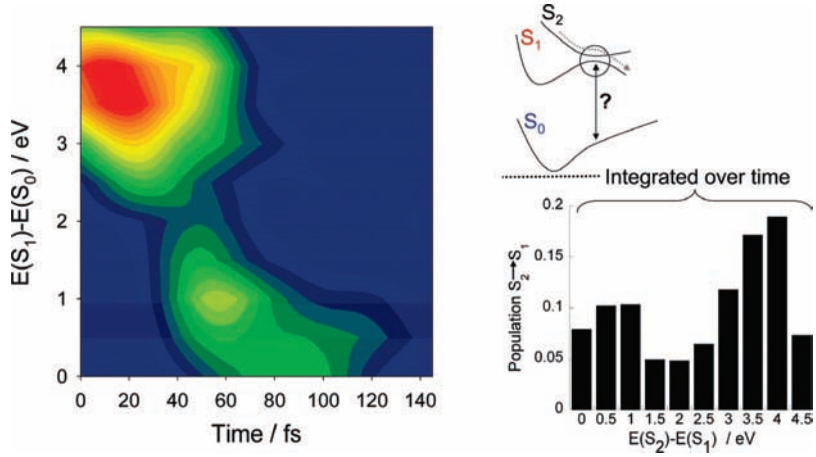

Figure 7. Left panel: Two-dimensional representation of $S_2 \rightarrow S_1$ nonadiabatic population transfer as a function of time and S_1/S_0 energy gap. Data have been convoluted in both dimensions as described in the text. Right panel: $S_2 \rightarrow S_1$ population transfer as a function of S_1/S_0 energy gap only, illustrating that most $S_2 \rightarrow S_1$ electronic relaxation occurs where the S_1/S_0 gap is 0.5 eV or greater.

dominant S_1/S_0 gap decreases as time progresses (left panel of Figure 7), signifying that the wavepacket is indeed approaching a region of 3-state intersections. The integrated plot (right panel of Figure 7) shows that there is a small amount of $S_2 \rightarrow S_1$ transfer (<10%) taking place at geometries with S_1/S_0 gaps of less than 0.5 eV. After this initial descent, S_1 population moves away from regions where the gap with S_2 is less than ~1 eV.

If population reaching S_1 passes quickly on to S_0, then promotion of direct $S_2 \rightarrow S_0$ decay by 3-state intersections is definitively established. Reversing the emphasis of Figure 7, where the property of interest was S_1/S_0 gaps at $S_2 \rightarrow S_1$ population transfer events, Figure 8 highlights S_2/S_1 gaps for $S_1 \rightarrow S_0$ events. Roughly 1% of the population is transferred to the ground state at points for which the S_2/S_1 gap is less than 0.5 eV (right panel of Figure 8), but the total distribution is concentrated at energy gaps in excess of 2 eV. Inspection of the time dependence (left panel of Figure 8) shows that population transferred at small gaps does so very early (50−100 fs) in time.

A brief examination of the S_1 surface provides some insight into the absence of direct decay from S_2 to the ground state. Figure 9 details S_1 surface extrema found at the CASSCF level, as well as MR-SDCI energy differences calculated at the CASSCF geometries (bold in the figure, given in parentheses below). The S_1 minimum, a planar and open geometry (i.e., the hydrogen bond length is considerably lengthened beyond that at the Franck−Condon point), lies roughly 1 eV (0.8 eV) below the hydrogen transfer transition state (C_2 symmetry), and almost 0.5 eV (0.2 eV) below the ME-3SI. The C_2 geometry is, in turn, more than 1 eV (0.8 eV) down from the HTI. Population passing from S_2 to S_1 near either of the two S_2/S_1 intersections (HTI or ME-3SI) will be funneled to the S_1 minimum or points lying lower in the S_1/S_0 intersection space (of which the S_1/S_0 MECI may be considered representative). In either case, the population is being funneled *away* from regions where the S_2/S_1 gap is small. Thus, direct relaxation from S_2 to S_0 is unlikely. The route to sequential $S_2 \rightarrow S_1 \rightarrow S_0$ relaxation that most *looks like* (and may be experimentally indistinguishable from) direct $S_2 \rightarrow S_0$ decay is then $S_2 \rightarrow S_1$ passage of a wavepacket traveling toward the ME-3SI followed by $S_1 \rightarrow S_0$ passage while the wavepacket travels away from the ME-3SI.

Trivial extension of an argument made by Mead and Truhlar provides qualitative justification for observing minimal direct $S_2 \rightarrow S_0$ relaxation. The original application[80] was to the frequency of conical intersections relative to that of purely avoided crossings (AC), contending that appearance of an AC probably indicates that a CI is somewhere nearby. The total configuration space volume spanned by $d = 3N - 6$ dimensions

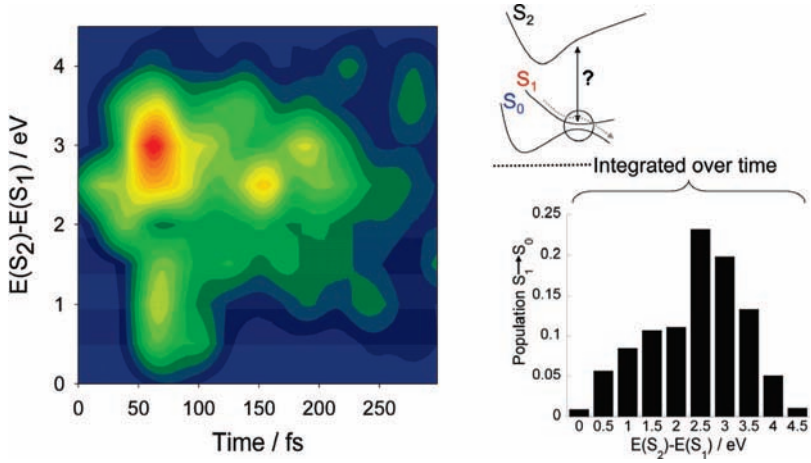

Figure 8. Left panel: Two-dimensional representation of $S_1 \rightarrow S_0$ nonadiabatic population transfer as a function of time and S_2/S_1 energy gap. Data have been convoluted in both dimensions as described in the text. Right panel: $S_1 \rightarrow S_0$ population transfer as a function of S_2/S_1 energy gap only, illustrating that all but a very small portion (<1%) occurs in regions where the S_2/S_1 gap is 0.5 eV or greater.

($N \geq 3$, where N is the number of atoms), each of linear extent L, is equal to L^d. The gap G separating a conically intersecting pair of adiabatic energy levels U_2 and U_1,

$$G \equiv U_2 - U_1 \tag{8}$$

is less than or equal to ϵ for a distance proportional to ϵ along each of the two branching plane directions (the gap grows linearly along these axes, and vanishes to first order along all others), so the "volume" occupied by each intersection in this region is $V_{CI} = L^{d-2}\epsilon^2$. By similar reasoning, the configuration space volume per 3-state intersection is $V_{3SI} = L^{d-5}\epsilon^5$.

The total volume consumed by conical intersections (3-state intersections) is then found by multiplying V_{CI} (V_{3SI}) by the total number of conical intersections (3-state intersections) within the full L^d region. Assuming a density ρ for zeros of electronic matrix elements gives rise to $N_{CI} = \rho^2 L^2$ and $N_{3SI} = \rho^5 L^5$. So the total ratio of configuration space volume consumed by 3-state intersections relative to that of conventional (2-state) intersections is

$$\frac{V_{tot}(3SI)}{V_{tot}(CI)} = \frac{N(3SI)V(3SI)}{N(CI)V(CI)} = \frac{(\rho^5 L^5)(L^{d-5}\varepsilon^5)}{(\rho^2 L^2)(L^{d-2}\varepsilon^2)} = (\rho\varepsilon)^3 \approx \varepsilon^3 \tag{9}$$

where the final, approximate, equality follows by assuming the density ρ to be $O(1)$, as rationalized previously.[80] This result is perfectly in keeping with the intuitive expectation that the distinction between 2- and 3-state intersections should be simply related to the difference in dimensionality (three) of their degenerate subspaces. Highlighted by this procedure, however, is the length scale dictating the precise magnitude of the difference—that defining the linear region surrounding the intersection seams. While no rigorous procedure currently exists for establishing bounds on the magnitude of ϵ, we estimate its order as 0.01 amu$^{1/2}$ Å on the basis of published values for previously characterized conical intersections.[49,81] Comparison with the ratio of two-state intersection volume to that of purely avoided crossings,

$$\frac{V_{tot}(AC)}{V_{tot}(CI)} \approx \varepsilon^{(d/2)-1} \tag{10}$$

reveals that (except in the case of very small molecules, and hence small values of d), the ratio of three-state to two-state intersection volumes is even smaller. It would not be surprising, then, to discover that three-state intersections were everywhere present but their *direct* effects nowhere visible.

We cannot presently exclude that the specific features of the potential energy surfaces in malonaldehyde may play a role in minimizing the direct effect of the three-state intersection. Thus, the generality of these results bears further investigation. However, it is important to note that our results do *not* imply that the indirect effects of three-state intersections are unimportant—the short lifetime of S_1 (approximately 100 fs from Figure 2) is due to the fact that the presence of the three-state intersection engenders large regions of closely spaced S_2/S_1 and S_1/S_0 intersections. Thus, the presence of a three-state intersection implies a higher probability than usual that population transferring from S_2 to S_1 (in the neighborhood of the three-state intersection) will come close to an S_1/S_0 intersection shortly thereafter. This *indirect* effect of three-state intersections is expected to be universal, since it depends only on simple topological considerations and the smoothness of the potential energy surfaces away from intersection seams.

5. Summary

Visualizing conical intersection seams in many-dimensional systems is challenging in any context, and is practically impossible without drastically restricting one's view to (at most) two-dimensional subspaces. The simplest solution, adequate for many purposes, is to characterize an extended region of the seam by its local minimum—at least in the sense that this geometry typifies, in some average way, those of the surrounding basin. This basin represents a locus of points at which nonadiabatic transitions concentrate. While this procedure can provide valuable guidance in building photochemical reaction pathways, it is equally conducive to the profoundly misleading impression that minimal energy points are somehow the whole story, dynamically speaking, or that they are necessarily relevant at all. Given that photochemical processes are by their very nature far from equilibrium, and most of the interesting molecules have many degrees of freedom, it can be quite difficult to make detailed predictions without extensive knowledge of the manner in which degenerate hypersurfaces (intersection spaces) criss-cross steepest descent lines and surface barriers. For processes where partial equilibration on the excited state precedes significant nonadiabatic effects, it is clear that the most insight will come from placement of intersection *seams* on *free* energy surfaces.[82−84]

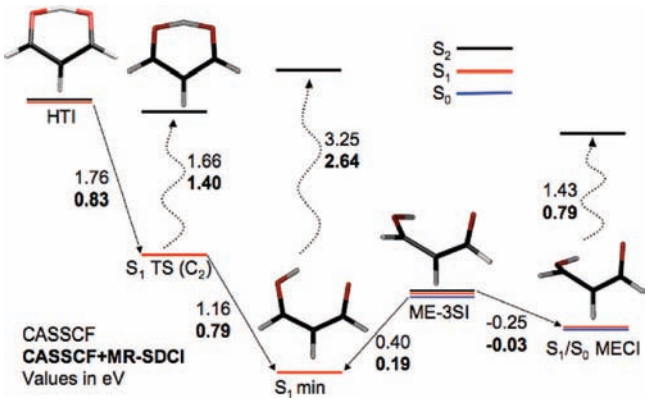

Figure 9. SA3-CAS(4/4)/6-31G* stationary points on the S_1 potential surface. Energy differences given in bold are taken from MR-SDCI energies calculated at the CASSCF-optimized geometries. Dotted arrows indicate energy gaps at a single geometry; straight arrows indicate energy differences for different geometries. Energy gaps with S_2 are large at both the S_1 minimum and the S_1/S_0 MECI, making it likely that pieces of the wavepacket arriving on S_1 from S_2 will be quickly funneled away from the region near the ME3CI. This decreases the likelihood of direct decay to S_0 through 3-state intersections. There is a large barrier to the (C_2) ESIPT transition state.

Many of the distinctive features of 3-state intersections, such as their consequences for geometric phase, remain an active area of research. We have provided a detailed look at nonadiabatic dynamics not only in the presence of a 3-state intersection, but one that constitutes the minimum energy point of the lowest spectroscopically accessible excited state (S_2). In spite of rapid ground state recovery, there is little evidence of direct $S_2 \rightarrow S_0$ population transfer. In addition, the vast majority (>95%) of population transferred between states does so at points for which the "complementary" gap (e.g., the S_2/S_1 gap in regions of $S_1 \rightarrow S_0$ relaxation) is large (>0.5 eV), signifying configuration space regions removed from the triply degenerate seam. Seam space dimensionality differences provide an intuitive rationale for this result, in that 3-state degeneracies are, to first order, broken in three dimensions additional (five, total) to those breaking 2-state degeneracies. Consequently, the latter persist over a much larger fraction of configuration space. To reach a 3-state intersection, wavepackets must weave their way through many 2-state intersections without losing all of their population. Even if a 3-state intersection is successfully reached from points higher in energy, the middle state must possess topography favoring rapid continuation to the next one lower in energy for direct transfer to occur. Nevertheless, three-state intersections are expected to have dramatic *indirect* effects in that their presence engenders many closely spaced two-state intersections and therefore greatly increases the likelihood of $S_2 \rightarrow S_1$ transfer followed quickly by $S_1 \rightarrow S_0$ transfer. This is suggested in the case of malonaldehyde by the very short (≈100 fs) lifetime of the intermediate S_1 state.

Evidence for the universality of intersection connectivity appears to be mounting. Given the machinery developed for seam following, it is possible to link chemically unrelated points in intersection spaces by pathways that may[33,36,37] or may not[45,49,81] follow steepest descent lines. Surprising examples of connectivity do not constitute proof, however, but provide motivation for a formal demonstration (or falsification) of the universal connectivity hypothesis.

Acknowledgment. This work was supported by the NSF through grants CHE-05-35640 and CHE-07-19291. J.D.C. thanks Dr. Seth Olsen for many helpful comments improving the style and readability of the manuscript.

References and Notes

(1) Brumer, P.; Shapiro, M. *Principles of the Quantum Control of Molecular Processes*; Wiley-Interscience: New York, 2003.
(2) Rice, S. A.; Zhao, M. *Optical Control of Molecular Dynamics*; Wiley-Interscience: New York, 2000.
(3) Martinez, T. J. *Acc. Chem. Res.* **2006**, *39*, 119.
(4) Balzani, V.; Clemente-Leon, M.; Credi, A.; Ferrer, B.; Venturi, M.; Flood, A. H.; Stoddart, J. F. *Proc. Natl. Acad. Sci.* **2006**, *103*, 1178.
(5) Brouwer, A. M.; Frochot, C.; Gatti, F. G.; Leigh, D. A.; Mottier, L.; Paolucci, F.; Roffia, S.; Wurpel, G. W. H. *Science* **2001**, *291*, 2124.
(6) Kamat, P. V. *J. Phys. Chem.* **2007**, *111C*, 2834.
(7) Born, M.; Oppenheimer, J. R. *Ann. Phys.* **1927**, *84*, 457.
(8) von Neumann, J.; Wigner, E. P. *Phys. Z.* **1929**, *30*, 467.
(9) Teller, E. *J. Phys. Chem.* **1937**, *41*, 109.
(10) Yarkony, D. R. *Acc. Chem. Res.* **1998**, *31*, 511.
(11) Yarkony, D. R. *Rev. Mod. Phys.* **1996**, *68*, 985.
(12) Baer, M.; Billing, G. D. The Role of Degenerate States in Chemistry. In *Advances in Chemical Physics*; J. Wiley & Sons: Hoboken, NJ, 2002; Vol. 124.
(13) Domcke, W.; Yarkony, D. R.; Koppel, H. *Conical Intersections: Electronic Structure, Dynamics, and Spectroscopy*; World Scientific Publishing Company: Hackensack, NJ, 2004.
(14) Levine, B. G.; Martinez, T. J. *Annu. Rev. Phys. Chem.* **2007**, *58*, 613.
(15) Matsika, S. *J. Phys. Chem.* **2005**, *109A*, 7538.
(16) Matsika, S.; Yarkony, D. R. *J. Chem. Phys.* **2002**, *117*, 6907.
(17) Matsika, S.; Yarkony, D. R. *J. Am. Chem. Soc.* **2003**, *125*, 10672.
(18) Matsika, S.; Yarkony, D. R. *J. Am. Chem. Soc.* **2003**, *125*, 12428.
(19) Coe, J. D.; Martinez, T. J. *J. Am. Chem. Soc.* **2005**, *127*, 4560.
(20) Coe, J. D.; Martinez, T. J. *J. Phys. Chem.* **2006**, *110A*, 618.
(21) Martinez, T. J. *Faraday Discuss.* **2004**, *127*, 227.
(22) Coe, J. D.; Levine, B. G.; Martinez, T. J. *J. Phys. Chem.* **2007**, *111A*, 11302.
(23) Chattoraj, M.; King, B. A.; Bublitz, G. U.; Boxer, S. G. *Proc. Natl. Acad. Sci.* **1996**, *93*, 8362.
(24) Domcke, W.; Sobolewski, A. L. *Science* **2003**, *302*, 1693.
(25) Tanner, C.; Manca, C.; Leutwyler, S. *Science* **2003**, *302*, 1736.
(26) Paterson, M. J.; Robb, M. A.; Blancafort, L.; DeBellis, A. D. *J. Phys. Chem.* **2005**, *109A*, 7527.
(27) Lochbrunner, S.; Wurzer, A. J.; Riedle, E. *J. Phys. Chem.* **2003**, *107A*, 10580.
(28) Herek, J. L.; Pedersen, S.; Banares, L.; Zewail, A. H. *J. Chem. Phys.* **1992**, *97*, 9046.
(29) Granucci, G.; Hynes, J. T.; Millie, P.; Tran-Thi, T. H. *J. Am. Chem. Soc.* **2000**, *122*, 12243.
(30) Aquino, A. J. A.; Lischka, H.; Hattig, C. *J. Phys. Chem.* **2005**, *109A*, 3201.
(31) Sobolewski, A. L.; Domcke, W. *J. Phys. Chem.* **1999**, *103A*, 4494.
(32) Bernardi, F.; Olivucci, M.; Robb, M. A. *Chem. Soc. Rev.* **1996**, *25*, 321.
(33) Migani, A.; Robb, M. A.; Olivucci, M. *J. Am. Chem. Soc.* **2003**, *125*, 2804.
(34) Ben-Nun, M.; Martínez, T. J. *Chem. Phys. Lett.* **1998**, *298*, 57.
(35) Weingart, O.; Migani, A.; Olivucci, M.; Robb, M. A.; Buss, V.; Hunt, P. *J. Phys. Chem.* **2004**, *108A*, 4685.
(36) Bearpark, M. J.; Blancafort, L.; Paterson, M. J. *Mol. Phys.* **2006**, *104*, 1033.
(37) Garavelli, M.; Page, C. S.; Celani, P.; Olivucci, M.; Schmid, W. E.; Trushin, S. A.; Fuss, W. *J. Phys. Chem.* **2001**, *105A*, 4458.
(38) Katriel, J.; Davidson, E. R. *Chem. Phys. Lett.* **1980**, *76*, 259.
(39) Han, S. S.; Yarkony, D. R. *J. Chem. Phys.* **2003**, *119*, 11561.
(40) Ichino, T.; Gianola, A. J.; Lineberger, W. C.; Stanton, J. F. *J. Chem. Phys.* **2006**, *125*, 084312.
(41) Schuurman, M. S.; Yarkony, D. R. *J. Phys. Chem.* **2006**, *110B*, 19031.
(42) Schuurman, M. S.; Yarkony, D. R. *J. Chem. Phys.* **2006**, *124*, 244103.
(43) Schuurman, M. S.; Yarkony, D. R. *J. Chem. Phys.* **2006**, *124*, 124109.
(44) Schuurman, M. S.; Yarkony, D. R. *J. Chem. Phys.* **2007**, *127*, 094104.
(45) Levine, B. G.; Coe, J. D.; Martinez, T. J. *J. Phys. Chem.* **2008**, *112B*, 405.
(46) Blancafort, L.; Robb, M. A. *J. Phys. Chem.* **2004**, *108A*, 10609.
(47) Kistler, K. A.; Matsika, S. *J. Chem. Phys.* **2008**, *128*, 215102.
(48) Han, S. S.; Yarkony, D. R. *J. Chem. Phys.* **2003**, *119*, 5058.
(49) Levine, B. G.; Ko, C.; Quenneville, J.; Martinez, T. J. *Mol. Phys.* **2006**, *104*, 1039.
(50) Fletcher, R. *Practical Methods of Optimization*, 2nd ed.; John Wiley & Sons: New York, 1987.
(51) Yarkony, D. R. *J. Phys. Chem.* **2004**, *108A*, 3200.
(52) Yarkony, D. R. *Faraday Discuss.* **2004**, *127*, 325.

(53) Laino, T.; Passerone, D. *Chem. Phys. Lett.* **2004**, *389*, 1.

(54) Sicilia, F.; Blancafort, L.; Bearpark, M. J.; Robb, M. A. *J. Chem. Theory Comput.* **2008**, *4*, 257.

(55) Roos, B. O. *Adv. Chem. Phys.* **1987**, *69*, 399.

(56) Docken, K. K.; Hinze, J. *J. Chem. Phys.* **1972**, *57*, 4928.

(57) Werner, H.-J.; Meyer, W. *J. Chem. Phys.* **1981**, *74*, 5794.

(58) MOLPRO, a package of ab initio programs designed by H.-J. Werner and P. J. Knowles, version 2002.1. Amos, R. D.; Bernhardsson, A; Berning, A.; Celani, P.; Cooper, D. L.; Deegan, M. J. O.; DobbynA. J.; Eckert, F.; Hampel, C.; Hetzer, G.; Knowles; P. J.; Korona, T.; Lindh, R.; Lloyd, A. W.; McNicholas, S. J.; Manby, F. R.; Meyer, W.; Mura, M. E.; Nicklass, A.; Palmieri, P.; Pitzer, R.; Rauhut, G.; Schütz, U; Schumann, U.; Stoll, H.; Stone, A. J.; Tarroni, R.; Thorsteinsson, T.; Werner, H.-J.

(59) Levine, B. G.; Coe, J. D.; Virshup, A. M.; Martinez, T. *J. Chem. Phys.* **2008**, *347*, 3.

(60) Heller, E. J. *J. Chem. Phys.* **1981**, *75*, 2923.

(61) Ben-Nun, M.; Martinez, T. J. *Adv. Chem. Phys.* **2002**, *121*, 439.

(62) Ben-Nun, M.; Quenneville, J.; Martínez, T. J. *J. Phys. Chem.* **2000**, *104A*, 5161.

(63) Szabo, A.; Ostlund, N. S. *Modern Quantum Chemistry*; Dover: Mineola, NY, 1996.

(64) Hillery, M.; O'Connell, R. F.; Scully, M. O.; Wigner, E. P. *Phys. Rep.* **1984**, *106*, 121.

(65) Bearpark, M. J.; Robb, M. A.; Schlegel, H. B. *Chem. Phys. Lett.* **1994**, *223*, 269.

(66) Barbatti, M.; Paier, J.; Lischka, H. *J. Chem. Phys.* **2004**, *121*, 11614.

(67) Bearpark, M. J.; Bernardi, F.; Olivucci, M.; Robb, M. A.; Smith, B. R. *J. Am. Chem. Soc.* **1995**, *118*, 5254.

(68) Coto, P. B.; Sinicrop, A.; De Vico, L.; Ferre, N.; Olivucci, M. *Mol. Phys.* **2006**, *104*, 983.

(69) Gomez, I.; Reguero, M.; Robb, M. A. *J. Phys. Chem.* **2006**, *110A*, 3986.

(70) Yarkony, D. R. *J. Chem. Phys.* **2005**, *123*, 204101.

(71) Seliskar, C. J.; Hoffmann, R. E. *Chem. Phys. Lett.* **1976**, *43*, 481.

(72) Arias, A. A.; Wasserman, T. A. W.; Vaccaro, P. H. *J. Chem. Phys.* **1997**, *107*, 5617.

(73) Paterson, M. J.; Bearpark, M. J.; Robb, M. A.; Blancafort, L. *J. Chem. Phys.* **2004**, *121*, 11562.

(74) Paterson, M. J.; Bearpark, M. J.; Robb, M. A.; Blancafort, L.; Worth, G. A. *Phys. Chem. Chem. Phys.* **2007**, *7*, 2100.

(75) Sicilia, F.; Blancafort, L.; Bearpark, M. J.; Robb, M. A. *J. Phys. Chem.* **2007**, *111A*, 2182.

(76) Sicilia, F.; Bearpark, M. J.; Blancafort, L.; Robb, M. A. *Theo. Chem. Acc.* **2007**, *118*, 241.

(77) Yarkony, D. R. *J. Chem. Phys.* **2005**, *123*, 134106.

(78) Tully, J. C. *J. Chem. Phys.* **1990**, *93*, 1061.

(79) Yarkony, D. R. *J. Phys. Chem.* **1997**, *101A*, 4263.

(80) Truhlar, D. G.; Mead, C. A. *Phys. Rev. A* **2003**, *68*, 032501.

(81) Lee, A. M. D.; Coe, J. D.; Ullrich, S.; Ho, M.-L.; Lee, S.-J.; Cheng, B.-M.; Zgierski, M. Z.; Chen, I.-C.; Martinez, T. J.; Stolow, A. *J. Phys. Chem.* **2007**, *111A*, 11948.

(82) Burghardt, I.; Cederbaum, L. S.; Hynes, J. T. *Faraday Discuss.* **2004**, *127*, 395.

(83) Burghardt, I.; Hynes, J. T. *J. Phys. Chem.* **2006**, *110A*, 11411.

(84) Burghardt, I.; Hynes, J. T.; Gindensperger, E.; Cederbaum, L. S. *Phys. Scr.* **2006**, *73*, C42.

JP806072K